Parametric Co-design of Machine-Inverter using Wide Band Gap and Three-level ANPC Inverter for 800V Traction System

Jaedon Kwak[1], and Alberto Castellazzi[2]
[1,2] Solid-State Power Processing Lab, Faculty of Engineering, Kyoto University of Advanced Science, Japan

***Abstract*-- This paper presents a methodology for the optimal co-design of an inverter and machine to enhance energy efficiency, considering the WLTC class 3 driving cycle. In the 800V system, a 3-level ANPC inverter and silicon carbide power devices are employed for the inverter design. These not only reduce energy consumption during the driving cycle but also significantly impact machine design parameters. A case study for an 800V traction system with a delta-shape IPMSM is presented. To optimize the inverter switching frequency, PWM strategy, and machine geometry, the DOE method is utilized, combined with FEM analysis. The results demonstrate an improvement in total energy loss during the drive cycle.**

Keywords—Energy loss consumption, 3-level ANPC, WBG-based inverter, 800V traction drive

I. INTRODUCTION

With the growing adoption of electric vehicles (EVs), extensive research has been conducted on high-voltage electric drive systems, such as 800V systems, to enhance driving range and battery charging speed. To fully capitalize on this transition from 400V to 800V systems, the development of an 800V-compatible electric powertrain is imperative. In the design of inverters, wide-bandgap (WBG) devices, which exhibit higher breakdown voltage and reduced switching losses compared to silicon (Si) devices, contribute to increased efficiency in electric drive systems [1, 2]. Multi-level inverters are well-suited for 800V systems due to their superior output waveform quality, characterized by low current ripple, and reduced voltage stress on each power device [3]. In addition, multi-level active neutral-point clamped (ANPC) inverters, which offer improved loss balancing compared to neutral-point clamped (NPC) inverters, can enhance the efficiency of traction system [4]. Various pulse-width modulation (PWM) strategies for 3-level ANPC inverters have been investigated, with the switching and conduction losses of each power device being influenced by the chosen PWM strategy [5, 6]. The most efficient PWM strategy can be determined, which is significantly affected by machine parameters and the main load conditions (load power factor, modulation index, and load current). Therefore, it is essential to accurately interpret the main load conditions, determine the optimal machine design variable, and assess the impact of the inverter PWM strategy, taking these factors into consideration. This paper presents a co-design methodology for inverter-machine systems in 800V high-voltage applications. Employing WBG devices and a 3-level ANPC topology, the optimal values of switching frequency and PWM strategy are investigated, considering the effects on the overall system through the use of design of experiments (DOE). Taking into account the interaction with inverter control characteristics, the complex geometric design optimization of delta-shaped interior permanent magnet synchronous machines (IPMSMs) is addressed to minimize the energy consumption during the Worldwide Harmonized Light Vehicles Test Cycle (WLTC) Class 3. Experimental validation of inverter efficiency considering load conditions is presented using rapid control prototyping (RCP) controller equipment.

II. CALCULATION ENERGY LOSS DURING DRIVE CYCLE

The initial design specifications for an 800V traction model are presented in Table I. To enhance energy efficiency, the total energy loss is calculated using the WLTC Class 3 cycle. Utilizing the vehicles specifications provided in Table II, the vehicle speed profile can be converted into a machine profile, represented by torque versus rotational speed. Fig. 1 illustrates the well-established longitudinal dynamic model used in vehicle dynamics to compute driving force (1)-(6), where F_{drive}, F_m, F_r, F_a, and F_c are driving force, acceleration force, rolling resistive force, aerodynamic drag force, and climbing force, respectively. Additional parameters are listed in Table II.

TABLE I
SPECIFICATION OF INITIAL 800V TRACTION MODEL

Item		Specification
Peak power / Torque		120kW / 195Nm
Nominal DC-link voltage		640Vdc
Max. speed		16,500 rpm
Inverter	Topology	2L-half bridge inverter with Si-IGBT
	Switching freq.	12kHz
Machine	Pole / Slot	8 / 48
	No. of series turns per phase	32 turns
	Winding type	Hair-pin rectangular wire

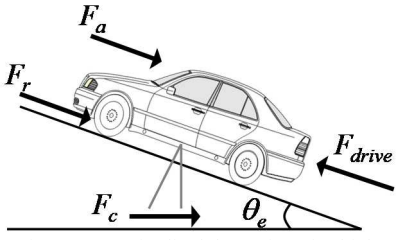

Fig. 1. Longitudinal dynamics of vehicle

TABLE II
SPECIFICATION OF VEHICLE MODEL

Item	Symbol	Units	Specification
Vehicle weight	M_v	kg	2050
Motor inertia	I	kg m^2	0.0025
Gear ratio	G	-	9.18
Gear efficiency	η_g	%	97
Tire dynamic radius	TDR	m	0.35
Rolling resistance coefficient	C_{rr}	-	0.008
Air drag resistance coefficient	C_d	-	0.21
Air density	ρ	kg/m^3	1.25
Frontal area	A_F	m^2	2.1
Vehicel speed	v	m/s	Profile
Acceleration	a	m/s^2	Profile
Regenerative brake ratio		%	70 (estimation)

$$F_{drive} = F_m + F_r + F_a + F_c \tag{1}$$

$$F_m = \left(M_v + \frac{I \cdot G^2 \cdot \eta_g}{TDR^2}\right) \cdot a \tag{2}$$

$$F_r = C_{rr} \cdot M_v \cdot g \cdot \cos\theta_e \tag{3}$$

$$F_a = \frac{1}{2}\rho \cdot A_F \cdot C_d \cdot v^2 \tag{4}$$

$$F_c = M_v \cdot g \cdot \sin\theta_e \tag{5}$$

$$\omega_m = v \cdot \frac{G}{TDR} \tag{6}$$

For improving design of traction system, considering all load points may introduce significant complexity and necessitate substantial computational resources and time. A more efficient optimization approach can be employed by utilizing representative points, which are determined through subregion division and energy gravity center calculations [7]. Fig. 2 depicts the machine profile and 10 representative points derived from the WLTC Class 3 cycle, obtained by applying the vehicle dynamic model.

III. IMPROVE DESIGN

A loss analysis is conducted at each 10 representative operating points to calculate total energy consumption and identify the optimal design by utilizing the co-simulation model depicted in Fig. 3 (a). Using the co-simulation model, the initial design concurrently considers not only the inverter design variables, such as PWM strategy and switching frequency, but also the expanded machine design variables arising from the use of WBG devices, all with the objective of achieving system energy reduction. In particular, the use of WBG devices enables the realization of higher switching frequencies, which in turn, enable the design of machines with increased pole numbers, ultimately facilitating the development of more efficient systems. The inverter model is designed using a 3-level ANPC topology with silicon carbide (SiC) devices, and two different topologies and corresponding two different PWM strategies are considered. The machine model is analyzed using the finite element method for designing an IPMSM, which typically exhibits high efficiency and power density. The JMAG-RT model is employed to account for the influence of inverter current, including harmonics, and machine losses and characteristics affected by the PWM control of the inverter. Following the initial design, the optimal design process is illustrated in Fig. 3 (b) using the DOE method.

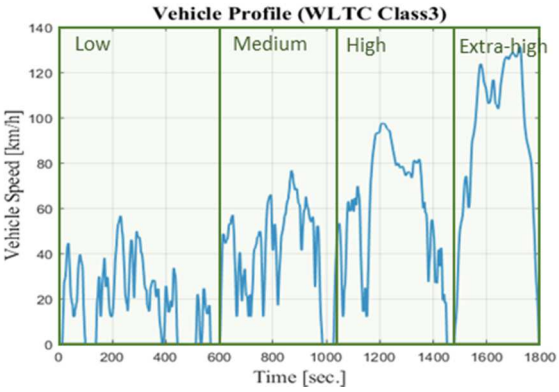

(a)

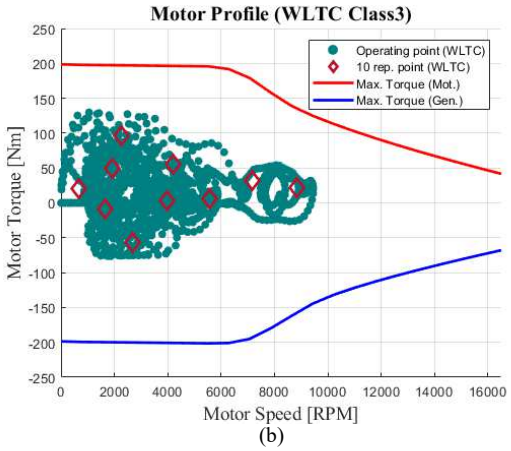

(b)

Fig. 2. WLTC Class 3 drive cycle (a) vehicle profile (b) machine profile and representative load point

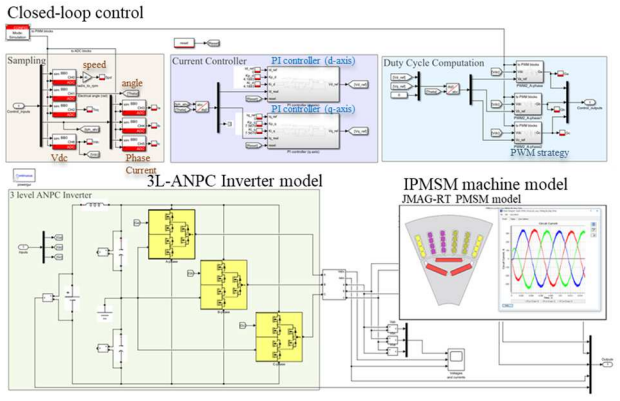

(a)

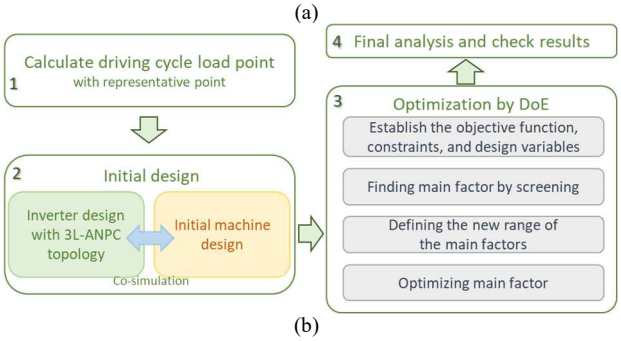

(b)

Fig. 3. (a) Co-simulation model for evaluating design (b) Optimal design process

A. *Inverter design with 3-level ANPC and SiC-MOSFET*

High-voltage systems require the use of power devices with higher voltage ratings. Conventional Si insulated-gate bipolar transistors (IGBTs) with ratings over 1200V exhibit increased losses due to the thicker drift layer of the power device. To minimize switching and conduction losses, SiC based metal-oxide-semiconductor field-effect transistors (MOSFETs) can serve as a suitable alternative. Moreover, employing multi-level topology allows for a reduction in voltage stress applied to each device, thereby enabling the use of power devices with lower voltage ratings. For an 800V system, using a 3-level ANPC reduces the voltage across each device between drain and source to 400V, allowing the application of SiC MOSFET rated at 650V. Fig. 4 illustrates two distinct topologies and corresponding two PWM strategies. Although cost may present a challenge, a more energy-efficient inverter can be achieved using all-SiC topology shown in Fig. 4 (a). In the hybrid topology, the PWM2 strategy can be adopted, which utilizes 4 Si-IGBTs/diodes and 2 SiC-MOSFETs, only two devices switch at high frequencies, as illustrated in Fig. 4 (b). SiC-MOSFETs are employed in these devices to reduce switching losses at high switching frequencies. As reported in [8], PWM2 is more suitable for high-speed, low-current regions where switching losses dominate. On the other hand, in the case of PWM1, the current path is distributed in parallel during zero-state, which results in a reduction of conduction losses. This proves advantageous in low-speed, high-current regions.

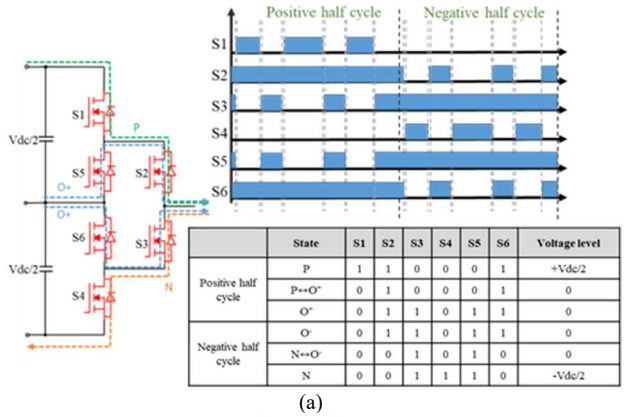

	State	S1	S2	S3	S4	S5	S6	Voltage level
Positive half cycle	P	1	1	0	0	0	1	+Vdc/2
	P↔O"	0	1	0	0	0	1	0
	O"	0	1	1	0	1	1	0
Negative half cycle	O'	0	1	1	0	1	1	0
	N↔O'	0	0	1	0	1	0	0
	N	0	0	1	1	1	0	-Vdc/2

(a)

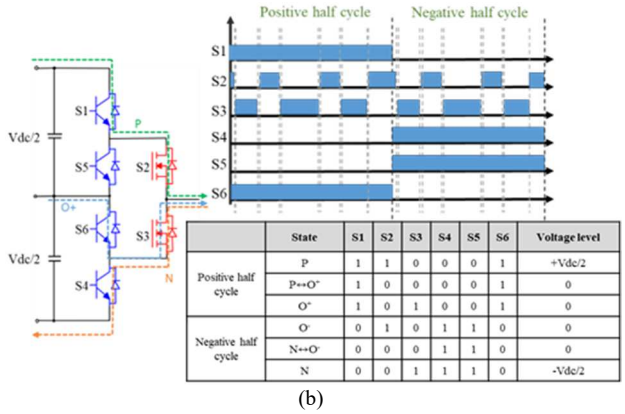

	State	S1	S2	S3	S4	S5	S6	Voltage level
Positive half cycle	P	1	1	0	0	0	1	+Vdc/2
	P↔O"	1	0	0	0	0	1	0
	O"	1	0	1	0	0	1	0
Negative half cycle	O'	0	1	0	1	1	0	0
	N↔O'	0	0	0	1	1	0	0
	N	0	0	1	1	1	0	-Vdc/2

(b)

Fig. 4. Two different PWM strategies and topologies (a) All-SiC topology and PWM1 schematics with current path (b) Hybrid topology and PWM2 schematics with current path

The current following through the devices of an ANPC exhibits considerable discontinuity. To calculate the loss, an average method is employed, with the effects of current ripple and deadtime being disregarded. Taking into account the load power factor φ, modulation index *m*, and power device data, conduction loss and switching loss can be determined using equations (7)-(10), where R_{on} represents the on-resistance, I_{pk} is the peak current in a single device, V_{DC} corresponds to the DC-link voltage, V_{ref} is the reference voltage of switching loss measurement, and f_s denotes the switching frequency. $s(\theta)$ is a switching function with a value of 0 or 1 when switch gate signal turn off and on respectively. The coefficients a, b, and c represent the switching on/off loss of the power device in (9). In Fig. 5, the phase angle between the modulation signal of S2 and phase current for both PWM1 and PWM2, the current of S2, and the gate signal are illustrated. In Fig. 5 (a), the conduction loss of S2 in the PWM1 strategy is calculated using integration range [φ, π+φ] for equation (7), and [0, φ] for equation (8). The modulation signal

$$P_{cond\_Q} = \frac{1}{2\pi}\int \left[R_{on}\left(I_{pk}\sin(\theta-\varphi)\right)^2 + V_0 I_{pk}\sin(\theta-\varphi)\right] s(\theta)d\theta \quad (7)$$

$$P_{cond\_D} = \frac{1}{2\pi}\int \left[R_{on}\left(-I_{pk}\sin(\theta-\varphi)\right)^2 - V_0 I_{pk}\sin(\theta-\varphi)\right] s(\theta)d\theta \quad (8)$$

$$E_{sw} = a\cdot I_d^2 + b\cdot I_d + c \quad (9)$$

$$P_{sw} = \left[\frac{1}{2\pi}\int \left[a\left(I_{pk}\sin(\theta-\varphi)\right)^2 + bI_{pk}\sin(\theta-\varphi) + c\right] d\theta\right]\frac{V_{DC}/2}{V_{ref}} f_s \quad (10)$$

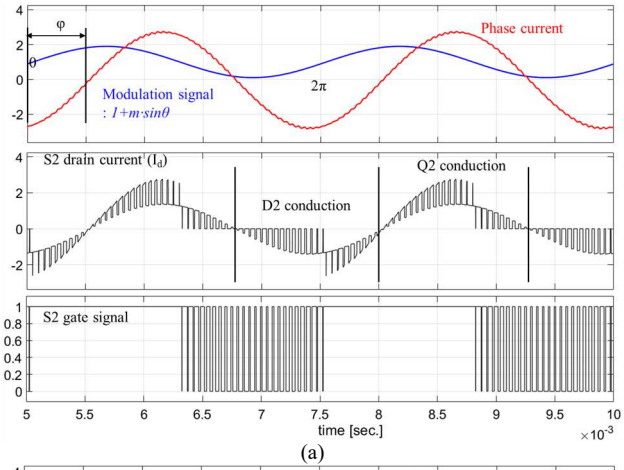

(a)

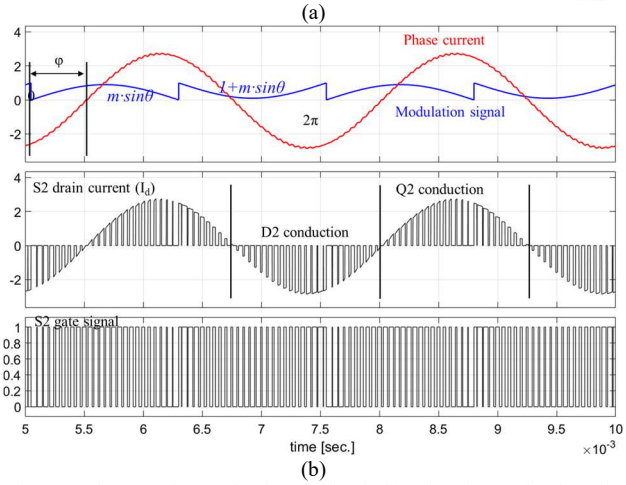

(b)

Fig. 5. Phase angle, conduction, and switching loss intervals of S2 for 3L-ANPC with different PWM strategies (a) PWM1 (b) PWM2

function is represented as $1+m \cdot sin\theta$. For the PWM2 strategy, the integration intervals are [φ, π] for positive half cycle, [π, π+φ] for negative half cycle of equation (7), and [0, φ] for positive, [π+φ, 2π] for negative half cycle of equation (8). In this case, the modulation signal is shown in Fig. 5 (b). In this manner, the conduction and switching losses for each device can be determined by defining the appropriate internals based on equation (7)-(10). In the simulation model, the losses can be calculated while considering the effect of deadtime and ripple.

B. Machine design with high switching frequency

The maximum desirable pole number is constrained by the maximum speed and inverter switching frequency. To ensure control stability even in extremely high-speed regions, the maximum designable pole number n_{p_max} is defined by (11), where N_{max} corresponds to the maximum operating speed, and m_f denotes the frequency modulation index.

$$n_{p\_max} = 120 \times \frac{f_s}{N_{max} \times m_f} \tag{11}$$

$$n_T = \frac{P_{max}}{3 i_{s\_max}} \cdot \frac{\sqrt{2}}{\pi^2} \cdot \frac{60}{\omega_m k_{w1} B_g D_r l_{stk}} \tag{12}$$

The number of series turns per phase, n_T, can be designed using (12), where P_{max} and i_{s_max} are the maximum power and root-mean-square (rms) phase current at base speed, respectively. The variable k_{w1} signifies the fundamental harmonic winding factor, while ω_m represents the mechanical base speed of the machine, and B_g, D_r, and l_{stk} denote the air-gap flux density, rotor outer diameter, and effective stack length, respectively. In hair-pin winding, the number of coils per slot must be even, which is one of its disadvantages. However, with higher inverter switching frequencies, a design with a greater pole number can be attained, which in turn enhances the range of achievable number of turns following the equation (11)-(12).

C. Preliminary experimental work of inverter

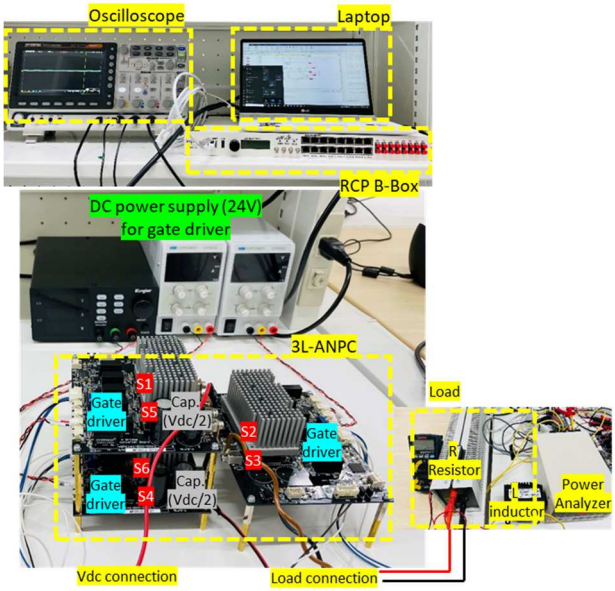

Fig. 6. Experimental setup : 3L-ANPC with SiC-MOSFET module connected by RCP controller

To validate the inverter loss and current ripple, experimental work is preliminarily conducted using a RCP controller setup. A prototype 3L-ANPC inverter model, composed of a SiC-MOSFET module, is connected to the RCP controller shown in Fig. 6. The RCP controller also facilitates real-time monitoring and debugging. By comparing the experimental results with simulation data for inverter loss and current ripple, the simulation model's accuracy can be verified. The full load condition with PWM1 and PWM2 will be conducted. Fig. 7 shows the output voltage and output current wave of PWM2 strategy with R-L load.

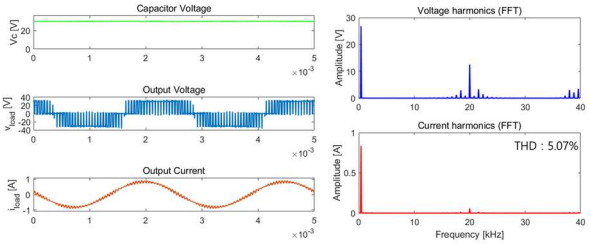

Fig. 7. Preliminary experimental results using PWM2 (f_s = 20kHz, f_1 = 400Hz, V_{DC} = 70V)

IV. Optimum Design with DOE

In the previous section, an initial improved design is developed, taking into consideration the interaction co-effect between the inverter and the machine. By utilizing SiC-MOSFET, a high switching frequency can be achieved, enabling the creation of a 10-pole machine while maintaining controllability even at 16,500 rpm. With a 10p/60s combination, the number of series turns per phase is designed as 40 turns, as described by equation (12). The detailed design for rotor and stator geometry is optimized in this section. Optimizing multiple parameters can be highly complex and demand significant computational effort. The DOE is a robust statistical technique that allows researchers to quantify the contribution of parameters to the objective function. The DOE method has been extensively studied for optimizing motor design, particularly in the context of geometric design [9, 10].

A. Design variables for inverter and machine

In the optimization process, six machine geometric design variables and two inverter variables are considered. Fig. 8 illustrates the initial configuration and the design variables for the machine. Starting from the initial value, a two-level low and high value range is provided in Table III.

TABLE III
Design Variables Initial Value and Variation Range

	Definition	Initial	Level Low	Level High
A	PWM strategy		PWM1	PWM2
B	Switching frequency (kHz)	30	20	40
C	Rotor diameter (mm)	122.5	120	125
D	Coil height (mm)	2.85	2.5	3.2
E	Pole arc1 ratio	0.47	0.4	0.5
F	Magnet 1 position	1.7	1.5	2.2
G	Pole arc2 ratio	0.82	0.75	0.85
H	Magnet 2 position	13	11	15

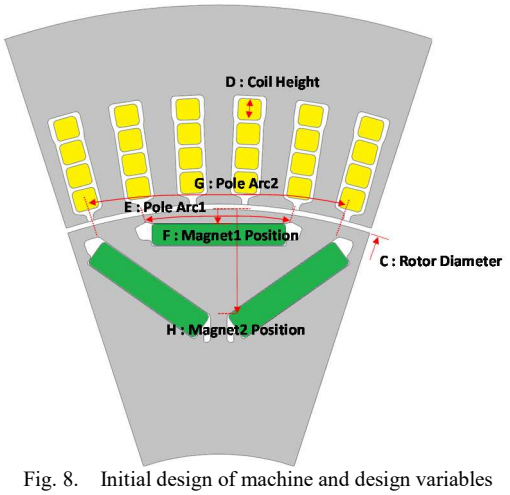

Fig. 8. Initial design of machine and design variables

The constraints are as follows:

- Fixed pole/slot combination
- Coil area is defined by constant current density; coil width is dependent on the coil height.
- Constant fill factor: < 58% (total bare copper area/slot area)
- Weight of magnet ≤ initial design (8p48s design)

B. Screening with fractional factorial design

Among the factors listed in Table III, some variables can significantly contribute to the objective function, while others have a very low dependency. In this study, a two-level, eight-factor fractional factorial design is employed to minimize the number of experiments. The objective function encompasses total loss, which consists of switching and conduction losses for the inverter, as well as copper, iron, and magnet eddy losses in the machine. These losses are analyzed at two different load points using a simulation model that incorporates FEM analysis for the machine and linked Simulink circuit analysis. The high-speed region and low-speed, high-torque point from among the 10 operating points have the most significant impact on total drive cycle loss. Utilizing a 1/16 fractional factorial design, $2^{(8-4)}$ experiments are conducted. Table IV presents the details of

TABLE IV
1/16 FRACTIONAL FACTORIAL DESIGN AND RESULTS

	Factor level combination	Loss @load1	Loss @load2
1	A1-B1-C1-D1-E1-F1-G1-H1	1615.9	843.2
2	A2-B1-C1-D1-E1-F2-G2-H2	1490.2	747.5
3	A1-B2-C1-D1-E2-F1-G2-H2	1621.4	733.3
4	A2-B2-C1-D1-E2-F2-G1-H1	1648.7	764.4
5	A1-B1-C2-D1-E2-F2-G2-H1	1338.5	689.7
6	A2-B1-C2-D1-E2-F1-G1-H2	1304.0	719.5
7	A1-B2-C2-D1-E1-F2-G1-H2	1369.7	645.2
8	A2-B2-C2-D1-E1-F1-G2-H1	1313.6	651.2
9	A1-B1-C1-D2-E2-F2-G1-H2	1622.9	789.8
10	A2-B1-C1-D2-E2-F1-G2-H1	1558.4	772.5
11	A1-B2-C1-D2-E1-F2-G2-H1	1655.9	825.7
12	A2-B2-C1-D2-E1-F1-G1-H2	1635.7	855.2
13	A1-B1-C2-D2-E1-F1-G2-H2	1809.9	849.4
14	A2-B1-C2-D2-E1-F2-G1-H1	1825.8	862.7
15	A1-B2-C2-D2-E2-F1-G1-H1	1907.4	768.5
16	A2-B2-C2-D2-E2-F2-G2-H2	1842.7	798.7

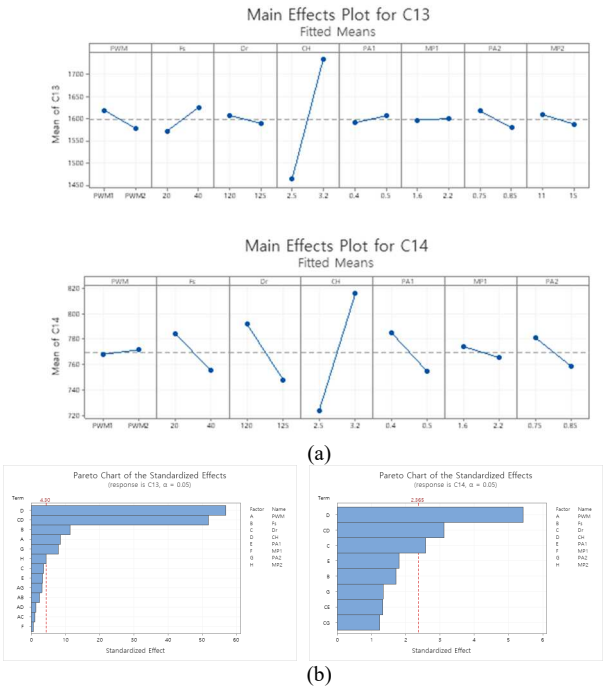

(a)

(b)

Fig. 9. (a) Mean plot of DOE for loss (b) Pareto chart for loss

the fractional factorial design and the results. Figure 5 illustrates: (a) the effect of each factor on loss at load1 and load2, and (b) Pareto charts for loss at load1 and load2. By pooling the non-effective factors, the Pareto chart is analyzed as shown in (b). For both load points, the most influential factors are C: rotor diameter and D: coil length. In this design, the contribution to loss from stator geometry is more significant than that from rotor geometry factors.

C. Optimizing main factor

In this study, the optimization of three main factors is analyzed based on the results of the fractional factorial design, while other factors are fixed in the direction for minimizing loss. Fig. 10 displays the direction of factors C and D for optimization. After further expanding the range of the high level for factor C and the low level for factor D, the response surface method (RSM) is employed. Utilizing a central composite design (CCD), a total of 15 (2^3+1+3×2) designs are analyzed. The optimized design values are presented in Table V.

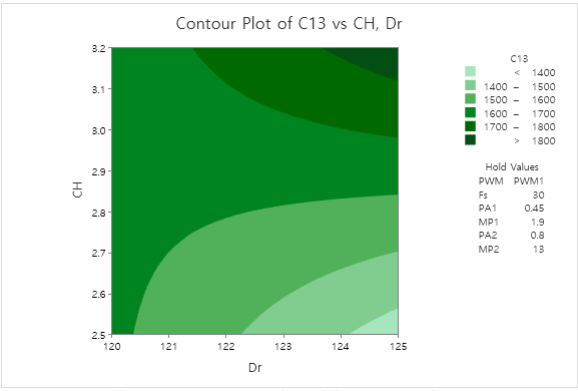

Fig. 10. Contour plot of factor C and D

TABLE V
FINAL OPTIMIZED DESIGN VALUE

	Definition	Optimized value
A	PWM strategy	PWM2
B	Switching frequency (kHz)	24
C	Rotor diameter (mm)	126.5
D	Coil height (mm)	2.47
E	Pole arc1 ratio	0.48
F	Magnet 1 position	2.2
G	Pole arc2 ratio	0.85
H	Magnet 2 position	15

D. Total energy loss during drive cycle for final design

Simulations are conducted for 10 representative points using the optimized design. By employing a hybrid topology 3L-ANPC with SiC-MOSFET and Si-IGBT, the total energy losses of the inverter can be reduced by 13.5%. For the machine design, an energy improvement of 6.4% can be achieved. Consequently, a 7.7% reduction in total energy loss during the driving cycle is observed.

TABLE VI
ENERGY LOSS CALCULATION OF IMPROVED DESIGN

Load point	Time [s]	Speed [rpm]	Torq. [Nm]	Energy loss [kJ]					
				Original			Improve		
				Inv.	Mach.	Total	Inv.	Mach.	Total
1	106	2185.2	99.7	41.5	134.8	176.2	31.2	127.5	158.7
2	127	6914.3	33.5	11.6	84.0	95.6	10.2	82.0	92.2
3	136	8537.4	22.9	8.5	80.0	88.5	8.5	81.2	89.7
4	138	4036.4	57.3	23.1	89.3	112.4	19.8	80.7	100.5
5	143	1857.4	52.2	21.2	59.3	80.5	20.4	51.4	71.8
6	149	2578.7	-58.2	24.8	76.8	101.6	21.5	69.7	91.2
7	193	5388.1	5.3	2.5	37.4	39.9	2.5	32.4	34.9
8	241	1620.8	-6.3	3.2	10.9	14.1	2.8	10.1	12.9
9	274	44.4	29.9	21.4	35.5	56.9	19.6	33.5	53.1
10	293	3828.0	3.0	1.9	30.7	32.6	1.6	29.5	31.1
Total energy loss during driving cycle [kJ]				159.6	638.6	798.2	138.1 (13.5%)	598.0 (6.4%)	736.1 (7.7%)

V. CONCLUSIONS

In this paper, a case study on an 800V electric vehicle (EV) traction machine and inverter is presented. For the 800V system, a 3L-ANPC topology and high switching frequency are designed, which impact the machine design process and design parameters, such as pole number and the number of series turns. Additionally, a hybrid topology and optimal PWM strategy are investigated, utilizing SiC-MOSFET and Si-IGBT as power devices. The inverter and machine parameters are simultaneously considered in the design process by implementing a co-simulation model. Moreover, a method for optimizing the machine's geometry and inverter parameters is introduced. To establish a specific design goal, the WLTC class 3 cycle is employed, which can be transformed into an electric drive profile based on the vehicle's specifications. Ultimately, the simulation results demonstrate a 7.7% reduction in total energy loss. This approach can be widely applied to the design of various electric drives.

REFERENCES

[1] A. Allca-Pekarovic et al., "Comparison of IGBT and SiC Inverter Loss for 400V and 800V DC Bus Electric Vehicle Drivetrains," 2020 IEEE Energy Conversion Congress and Exposition (ECCE), 2020, pp. 6338-6344.

[2] W. Taha et al., "Efficiency Evaluation of 2L and 3L SiC-Based Traction Inverters for 400V and 800V Electric Vehicle Powertrains," 2021 IEEE Transportation Electrification Conference & Expo (ITEC), 2021, pp. 625-632.

[3] A. Kersten, E. Grunditz and T. Thiringer, "Efficiency of Active Three-Level and Five-Level NPC Inverters Compared to a Two-Level Inverter in a Vehicle," EPE'18 ECCE Europe, 2018, pp. P.1-P.9.

[4] H. Messaoudi et al., "Thermal performance-based comparative study of PWM strategies for three-level ANPC converter," 2016 7th International Renewable Energy Congress (IREC), 2016, pp. 1-6.

[5] M. Novak, V. Ferreira, F. Blaabjerg and M. Liserre, "Evaluation of carrier-based control strategies for balancing the thermal stress of a hybrid SiC ANPC converter," *2021 IEEE Applied Power Electronics Conference and Exposition (APEC)*, Phoenix, AZ, USA, 2021, pp. 2077-2083.

[6] N. K. Muthukuri and R. Tagore Yadlapalli, "Comparison of carrier based PWM technique for Active Neutral Point Clamping Multilevel Inverter," *2020 4th International Conference on Intelligent Computing and Control Systems (ICICCS)*, Madurai, India, 2020, pp. 1288-1292.

[7] Dong Wei, Hongwen He, Jianfei Cao, "Hybrid electric vehicle electric motors for optimum energy efficiency", A computationally efficient design, Energy, Vol. 203, 2020.

[8] J.D. Kwak, A. Castellazzi, "Inverter-machine parametric co-design for energy efficient electric drives," in *Proc. EPE'22 ECCE Europe*, Sep. 2022.

[9] Cui, Junguo & Xiao, Wensheng & Zou, Wenqiang & Liu, Simiao & Liu, Qi., "Design optimization of submersible permanent magnet synchronous motor by combined DOE and Taguchi approach", *IET Electric Power Applications 14*, 2020.

[10] C. -C. Hwang, C. -T. Liu and C. J. Hong, "Optimal design of an IPM motor using fuzzy-based Taguchi method and Rosenbrock's algorithm," *2016 XXII International Conference on Electrical Machines (ICEM)*, 2016, pp. 1957-1962.